Technological Advancement

Fourier-based spatial mapping of oscillatory phenomena in fungi

M.D. Fricker [a],*, M. Tlalka [a], D. Bebber [a], S. Tagaki [b], S.C. Watkinson [a], P.R. Darrah [a]

[a] *Department of Plant Sciences, University of Oxford, South Parks Road, Oxford OX1 3RB, UK*
[b] *Research Institute for Electronic Science, Hokkaido University, Sapporo 060-0812, Japan*

Abstract

Microorganisms display a range of oscillatory phenomena that operate over different temporal scales. Fourier analysis provides a compact description of such oscillations in terms of their frequency, magnitude and phase. However, in the majority of studies there is no explicit consideration of the spatial organisation of the oscillation. Here we describe procedures and a software package to map oscillatory phenomena in microorganisms in both the time and frequency domains. Key parameters of interest, such as frequency, phase or magnitude of the oscillations, are presented as pseudo-colour coded maps. This maintains the spatial information in the image and greatly facilitates understanding of potentially complex propagating waves or development of oscillatory domains with distinct behaviour. We illustrate the utility of this system with reference to spatial analysis of the pulsatile component to amino acid transport in mycelial systems of *Phanerochaete velutina* and *Coniophora puteana*, and actin–myosin based contractions in *Physarum polycephalum*.
© 2007 Elsevier Inc. All rights reserved.

Keywords: Fourier analysis; Phase domain; Metabolic oscillation; Self-organisation; Hilbert transform

1. Introduction

Microorganisms display a range of rhythmic phenomena with different periods ranging from ultradian metabolic and transcriptional oscillators in yeast (Kippert, 2001; Lloyd and Murray, 2005; Lloyd, 2006; Reinke and Gatfield, 2006), through pulsatile growth of *Physarum* (Ueda, 2005), cAMP-dependent signalling waves during aggregation in *Dictyostelium* (Sawai et al., 2005; Dormann and Weijer, 2006), to the canonical temperature-compensated circadian oscillators in *Neurospora* (Lakin-Thomas and Brody, 2004; Bell-Pedersen et al., 2005; Dunlap, 2006; Lakin-Thomas, 2006a; Lakin-Thomas, 2006b; Liu and Bell-Pedersen, 2006). When there is no explicit spatial dimension to the oscillation, analysis of the rhythm can be captured by the average response of the system and presented as a simple graph of the time-series (Priestley, 1981; Diggle, 1990; Smith, 1997; Chatfield, 2004), provided the

sampling interval itself does not introduce aliasing artifacts (Gilbert and Ferreira, 2000). However, visualisation and analysis of oscillatory systems in two (or even three) dimensions is more challenging (see for example Aon et al., 2007). Whilst it is possible to present a number of time-series graphs for different regions-of-interest (ROIs), this can only capture a very small sub-set of the total oscillatory behaviour. This approach is progressively less useful as the spatial complexity of the rhythmic behaviour increases. An alternative strategy is to analyse the image series in the frequency domain and summarise the oscillatory behaviour by particular key attributes, such as the frequency, phase or magnitude (Visser et al., 1990; Gilbert and Visser, 1993; Tlalka et al., 2002; Tlalka et al., 2003; Roussel and Lloyd, 2007). This approach can be extended to a pixel-by-pixel analysis in which the frequency, phase or magnitude are represented as the hue in pseudo-colour coded images. This maintains the spatial information in the image and greatly facilitates understanding of potentially complex propagating waves or development of oscillatory domains with distinct behaviour (see for example Gray et al., 1998; Mrsic-Flogel et al., 2003; Sawai et al., 2005).

---

* Corresponding author. Fax: +44 0 1865 275074.
  E-mail address: mark.fricker@plants.ox.ac.uk (M.D. Fricker).

Here we describe a set of general procedures and a software package to perform spatial mapping of oscillatory phenomena in both time and frequency domains for microbial systems. We illustrate the utility of this approach by reference to spatial analysis of the pulsatile component of amino acid transport in mycelial systems of *Phanerochaete velutina* (Tlalka et al., 2002; Tlalka et al., 2003) and *Coniophora puteana*. The approach is a generic one and is suitable to any image series in which the oscillatory behaviour is present as changes in image intensity. To illustrate this point we also present analysis of rhythmic actin–myosin based contractions in *Physarum polycephalum* (Ueda, 2005).

2. Materials and methods

2.1. Imaging radiolabelled nutrient movement in saprotrophic fungi

Cultures of *P. velutina* and *C. puteana*, originally isolated from the field by Prof. L. Boddy (Cardiff University), were maintained on 2% malt agar (2% Oxoid malt extract, 2% Oxoid No. 3 agar) at 22 ± 1 °C in darkness in a temperature-controlled incubator (Gallenkamp, England) as previously described (Tlalka et al., 2002; Tlalka et al., 2003). Transport of $[^{14}C]$-amino-isobutyrate ($[^{14}C]$-AIB)[1] or $[^{14}C]$-O-methyl glucose ($[^{14}C]$-OMG) was visualised by photon-counting scintillation imaging in colonies grown across a BioMax TranScreen LE intensifying screen (Sigma, Poole, UK) from a 12 mm inoculum plug in the presence or absence of additional cellulose bait (13 mm disc, Grade AA filter paper, Whatman, Maidstone, England) using a high-resolution, photon-counting camera system (HRPCS-3, Photek Inc., St. Leonards on Sea, UK) as described previously (Tlalka et al., 2003). For most experiments, 20 µl (37 kBq) of a 0.9 mM solution of 2-amino[1-^{14}C]isobutyric acid, $[^{14}C]$-AIB, specific activity 2.11 GBq mmol^{-1} (Amersham, UK) in 2% v/v EtOH was applied to the inoculum. The chambers were sealed and imaged in a temperature-controlled room at 19–22 °C, monitored with "Diligence"™ data loggers (Comark Ltd., UK). Temperatures for individual experiments were kept to ±0.5 °C. Images were integrated over 60 min and experiments lasted up to 400 h.

2.2. Imaging actin–myosin contractions in Physarum polycephalum

Movies of the evolution of rhythmic contraction patterns in *P. polycephalum* were collected by bright field time-lapse imaging. In brief, plasmodia of *P. polycephalum* (strain HU195 × HU200) were grown on a 1% agar at 23°

in the dark and fed with oat meal (Ueda, 2005). Growth was constrained within ∼2.5 cm wide channels using acetate sheet. Alternatively, small volumes of endoplasm, typically 1 µl, were collected using a glass capillary, following puncture of a vein in the large plasmodium. Endoplasmic drops around 0.9 mm diameter were placed on a 1.5% agar plate and observed under dissecting microscope (Nikon SMZ-1500, Nikon, Tokyo, Japan) with bright field illumination. The motion of the plasmodium was visualised with a cooled CCD video camera (Retiga EXi Fast 1394 Mono Cooled, Qimaging, Burnaby, BC, Canada) and digitised at 696 × 520 pixel resolution into 12 bit image series at 3–4.2-s intervals.

2.3. Analysis of the oscillatory component

Movie files in *avi* format were exported from each experimental system, imported into the MatLab environment (The Mathworks, Inc., Natick, MA, USA) and analysed using Fourier techniques on a pixel-by-pixel basis. Full details of the results of these manipulations and their justification are given in the results section. The software is available as a stand-alone package on request from the authors.

3. Results and discussion

We have previously shown that transport of the amino-acid analogue, $[^{14}C]$-aminoisobutyrate ($[^{14}C]$-AIB) through colonies of *P. velutina* showed a pulsatile component superimposed on an overall accumulation at the growing margin (Tlalka et al., 2002; Tlalka et al., 2003). In microcosms with an additional cellulose resource (Fig. 1A), the pattern of distribution and oscillation was more complex. Label preferentially accumulated in the sector of the colony containing the bait (Fig. 1A and B), and measurements from specific regions of interest (ROIs) revealed that different domains within the colony all pulsed, but were not necessarily in phase with each other. However, even with repeated sampling from different ROIs, it was extremely difficult to build up a picture of how these oscillations were organised or propagated over the whole colony by simple comparison of traces over time. Thus, to determine whether the oscillations were organised into domains with locally synchronized behaviour within the colony, we extended our previous Fourier analysis (Tlalka et al., 2002; Tlalka et al., 2003) to every pixel in the discrete time-series and displayed the results as pseudo-colour coded maps of frequency, magnitude and phase (Fig. 1). These images provided an immediate representation of the key parameters defining the oscillation.

The scintillation image series were noisy (Fig. 1A and C) and required smoothing in either the (x, y) plane or over time or both. Simple square or Gaussian averaging filters with kernel sizes of 3–7 pixels worked well and were easy to implement (Fig. 1D). More sophisticated polynomial or spline regression approaches were also examined, but

---

[1] *Abbreviations used:* AIB, aminoisobutyrate; DFT, discrete Fourier transform; HSB, hue, saturation brightness colour space; OMG, *O*-methyl glucose; PCSI, photon-counting scintillation imaging; RGB, red, green, blue colour space.

in the absence of an underlying theoretical model to explain the trend (Priestley, 1981; Chatfield, 2004), most analyses were conducted with simple moving averages. Smoothing in the time-domain corresponds to a low pass filter that removed high frequencies from the analysis. Typically, the length of the moving average kernel in time was selected to be around 25% of the period of the major oscillation observed.

Oscillations superimposed on different long-term trends were clearly seen in the smoothed data (Fig. 1D). It was also apparent that the oscillations were not in-phase for samples taken from the inoculum, added resource or foraging cord. It was less clear whether these differences were consistent features of each functionally distinct region, or varied widely across the colony. Rather than repeated sampling using multiple ROIs and comparing traces in the time-domain, the oscillation for each pixel in the time-series was characterised using Fourier analysis and summarised by its dominant frequency, phase and magnitude.

Fourier analysis requires a stationary time-series with a mean of zero (Priestley, 1981; Diggle, 1990; Chatfield, 2004). However, the oscillatory behaviour of interest was superimposed on relatively strong underlying trends arising from increasing time-dependent uptake and transport of [14C]-AIB around the colony (Fig. 1D). Thus the trends had to be removed before the data was suitable for further analysis. De-trending was achieved by either repeatedly taking the difference of adjacent points in the time-series until the series appeared stationary, or subtracting an estimate of the trend derived from a simple moving average with an order that matched the period of the oscillation (Fig. 1E, Priestley, 1981; Diggle, 1990; Smith, 1997; Chatfield, 2004). Choosing the correct order took two or more iterations as the appropriate period for de-trending required knowledge of the period of the oscillations.

In many cases, the trend itself contained useful biological information. For example, in the case of [14C]-AIB transport, the trend gave a measure of the rate and magnitude of [14C]-AIB accumulation in different parts of the colony. In situations where the tracer was added to a pre-grown colony, the time at which the trend increased more than 2 SD above the local background provided an objective measure of the time-of-arrival (ToA) of the amino-acid (Fig. 1L). If the label was present at the start of growth and accumulated at the colony margin, a radial profile across the ToA image provided a graphical representation of the colony growth. If the label was added to an existing network, profiles along morphological features in the ToA image, such as a cord, should provide an estimate of the rate of amino-acid transport, with the first derivative of these profiles giving the local velocity of the corresponding process. In practice, the signal-to-noise (S/N) ratio from these scintillation images was usually too low and the sampling interval (1 h) too long in comparison with the rate of amino-acid movement through the cords to give reliable results (data not shown). Nevertheless, the software includes the facility to extract user-defined profiles across the raw and processed image series, and to extract the ToA profile for experimental situations when the S/N ratio is better.

3.1. Analysis of the oscillatory component using Fourier techniques

Subtraction of the trend provided an oscillation centered about zero (Fig. 1F). Depending on the type of oscillation, it was sometimes appropriate to normalise by the trend at each time point to express the oscillation as a proportion of the total signal. This approach highlighted areas where a substantial fraction of the signal was oscillating, irrespective of the overall intensity. Normalisation also compensated for any unwanted signal attenuation. For example, in the case of [14C]-AIB transport, attenuation of the scintillation signal by the inoculum plug or added resource decreased the total signal detected by a factor of 2–3-fold (Fig. 1A and B), but did not obscure the relative proportion of the signal that was oscillating.

During calculation of a discrete Fourier transform (DFT), the de-trended signal is treated as though it were periodic. In practice, the sample of the time-series did not correspond to an integral number of complete cycles starting at zero, and therefore had abrupt transitions at the start and end of the series where the data was truncated (Fig. 1F). To avoid the introduction of spurious high frequency components to match these artificial transitions, the time-series was filtered with a well defined window function to reduce the contribution of samples at either end of the signal (Fig. 1G, Priestley, 1981; Diggle, 1990; Smith, 1997). A number of different windowing functions were tested that offered different compromises between broadening of the main Fourier peak, reducing the amplitude of the tails and quantitatively preserving the magnitude of the dominant Fourier frequency (Smith, 1997). Typically we used a Hanning or Blackman window as a reasonable compromise between these different criteria (Fig. 1G).

As many experimental time-series were short with relatively few cycles, the Fourier spectrum lacked resolution and the finite length of the data series gave rise to spectral leakage with broadening of the main peak (Chatfield, 2004). Thus without further adjustment, the fundamental Fourier frequency was constrained by the length of the data to one cycle in N data points, and the oscillations then partitioned amongst a limited number of integer multiples, or harmonics, up to the Nyquist limit of twice the sampling period. Often the main frequency of the oscillation apparent in the time-series plots was not necessarily present as one of the Fourier basis functions, but fell between adjacent frequencies. Improved resolution of the peak frequency was achieved by padding the windowed series with zeros (Smith, 1997), typically to lengths that were powers of 2 to speed up calculation of the DFT. For example, the typical period for [14C]-AIB transport ranged from

12 h to 16 h in *P. velutina* (Tlalka et al., 2002; Tlalka et al., 2003), thus a signal digitised at 1 h intervals and lasting 128 h gave relatively coarse resolution of this peak Fourier frequency (FF) as FF 8, 9 and 10, corresponded to periods of 16 h, 14.2 h and 12.8 h, respectively. Increasing the padding to 256 samples introduced two additional Fourier frequencies in this range, corresponding to periods of 15.1 h and 13.5 h, increasing the probability that the "true" frequency of the oscillation would coincide with one of the discrete Fourier frequencies in the analysis. Clearly, more padding gives increasingly fine resolution of the spectrum, but at the expense of computational time and memory storage.

In theory the highest frequency oscillations that can be studied by this approach are determined, not by the resolution of the Fourier spectrum, but by the Nyquist limit defined as twice the sampling period. In practice, the risk of aliasing artifacts increases markedly when the observed frequencies are close to this limit (Gilbert and Ferreira, 2000), so we preferred to use a sampling frequency several fold higher than the observed frequency. For example, the sampling integration period was 1 h for [^{14}C]-AIB transport in *P. velutina* and *C. puteana*, with a temporal smoothing of 5 h, in comparison to an oscillation period of ∼14 h and ∼25 h, respectively. However, in the case of *Coprinus picaceous*, the oscillation had a period of 4 h, so the sampling integration period was reduced to 30 min and no temporal averaging was used (data not shown).

The DFT decomposes the time-domain signal into arrays of pure sine and cosine waves at each Fourier frequency. It was more convenient to convert these into polar form as arrays of magnitude and phase for each Fourier frequency, as these provided a direct readout of the main parameters of biological interest (Fig. 1J,K). 2-D arrays of these values for each pixel at the peak Fourier frequency

(Fig. 1M) were mapped across the spatial field and pseudo-colour coded with appropriate scaling (Fig. 1N and O). In the case of the magnitude, the value of the peak only accurately reflected the amplitude of the oscillation if the natural frequency of the oscillation fell precisely on one of the Fourier basis functions. However, the magnitude or power of just the peak was difficult to interpret directly as both the shape of the oscillation and the extent of pre-processing almost invariably distributed the power across a number of adjacent Fourier frequencies. Thus if quantitative estimates of the amplitude of the oscillation were needed, we preferred to use the instantaneous magnitude derived from the Hilbert transform, which also captures the temporal evolution of the oscillation in a more intuitive form (see below).

Phase comparisons across the image only make sense for oscillations that have the same frequency. Thus pixels outside a limited frequency tolerance range, typically ±1 from the peak Fourier frequency from the padded data series, were excluded from the pseudo-colour representation. These regions were then displayed in greyscale to retain an impression of their morphology (Fig. 1O). Typically such regions occurred at the growing margins, where the dramatic increase in signal as the growing margin or transport front passed across a pixel initially swamped the contribution from the subsequent oscillatory behaviour and gave the Fourier spectrum a more complex form. To facilitate comparison between experiments, it was convenient to express the phase on a rainbow spectrum, tuned so that particular reference regions, such as the inoculum, had the same initial colour. The colour scale then ran from ±π radians or ±180°, but was also annotated with the period in hours. This visually focussed attention on the relative phase relationship between different regions, but also allowed cross-reference to the absolute phase difference in hours.

Fig. 1. Flow diagram of the steps involved in mapping the frequency, phase and magnitude of oscillatory phenomena. Images of [^{14}C]-AIB movement were recorded by photon-counting scintillation imaging of colonies of *Phanerochaete velutina* (A). The overall distribution of label was summarised as an average projection over time for the whole image series (B). The signal-to-noise ratio for each pixel was improved by a combination of spatial averaging in the (x, y) plane, using a 5×5 or 7×7 pixel kernel, and temporal averaging over a moving 3 h or 5 h window for each pixel. Data from three individual pixels shown in (B) are presented in (C) and (D) to illustrate the effect of these manipulations. The longer term trends in the data were isolated using a 12–18 h moving average (E), selected to match the period of the oscillations. The oscillatory component was isolated by subtracting the trend data from the smoothed data to give a stationary series suitable for Fourier analysis (F). To minimise the effects of abrupt transitions at the end of the time-series, data were smoothed with a Hanning window of the same length as the data (G). If necessary, the array containing the oscillation data was padded with zeros along the time axis to reach the next integer power of 2, typically 128 or 256. The instantaneous magnitude (H) and phase (I) were calculated using the Hilbert transform to provide an indication of the temporal evolution of the oscillation, particularly the envelope of the amplitude (H). The discrete Fourier Transform (DFT) was calculated on a pixel-by-pixel basis to give arrays of magnitude (J) and phase (K) for each pixel. The dominant Fourier frequency with the maximum magnitude was determined for each pixel and the corresponding phase and magnitude images were extracted from these arrays. Colour representations of each Fourier variable were constructed in HSB (hue, saturation, brightness) colour space with the parameter of interest, coded as hue, the intensity coded as the average intensity for each pixel in the time-series, and the saturation set at maximum for all pixels. The HSV images were converted to RGB colour space for display. The pulsatile component of transport showed the same frequency throughout most of the colony (M), equivalent to a period of 14.3 h in this case. Regions with different frequency and the growing margins, where the advancing front disrupted the Fourier analysis, were coded in greyscale and excluded from further analysis. Results were displayed as pseudo-colour coded maps of the magnitude (N) and phase (O) at the dominant Fourier frequency. The oscillations showed clearly demarcated domains with high magnitude (N), but different phase (O) in the inoculum and bait, corresponding to a ∼3 h phase difference. There was a greater phase shift in the connecting cord (∼5 h), whilst the rest of the mycelium was synchronised, but even further out-of-phase (6–7 h). To map the spread of the label throughout the network, the time when the signal rose higher than the mean plus $2 \times SD$ of the background level was also determined. In this example, the time of arrival image (L) shows that [^{14}C]-AIB movement was initially directed to the left of the colony and gives a signal early in the time course (red). Addition of the bait was accompanied by increased growth along the top and right margins, giving a signal later in the time course coded blue.

3.2. Analysis of the temporal evolution of the oscillation using the Hilbert transform

The Hilbert transform provides the instantaneous magnitude and phase of the signal for each time point in a time-series (Huang et al., 1999). It is therefore less useful than the Fourier approach to provide a single summary value capturing the essence of the oscillation, but provides a more detailed view of the temporal evolution of the oscillation. The instantaneous magnitude
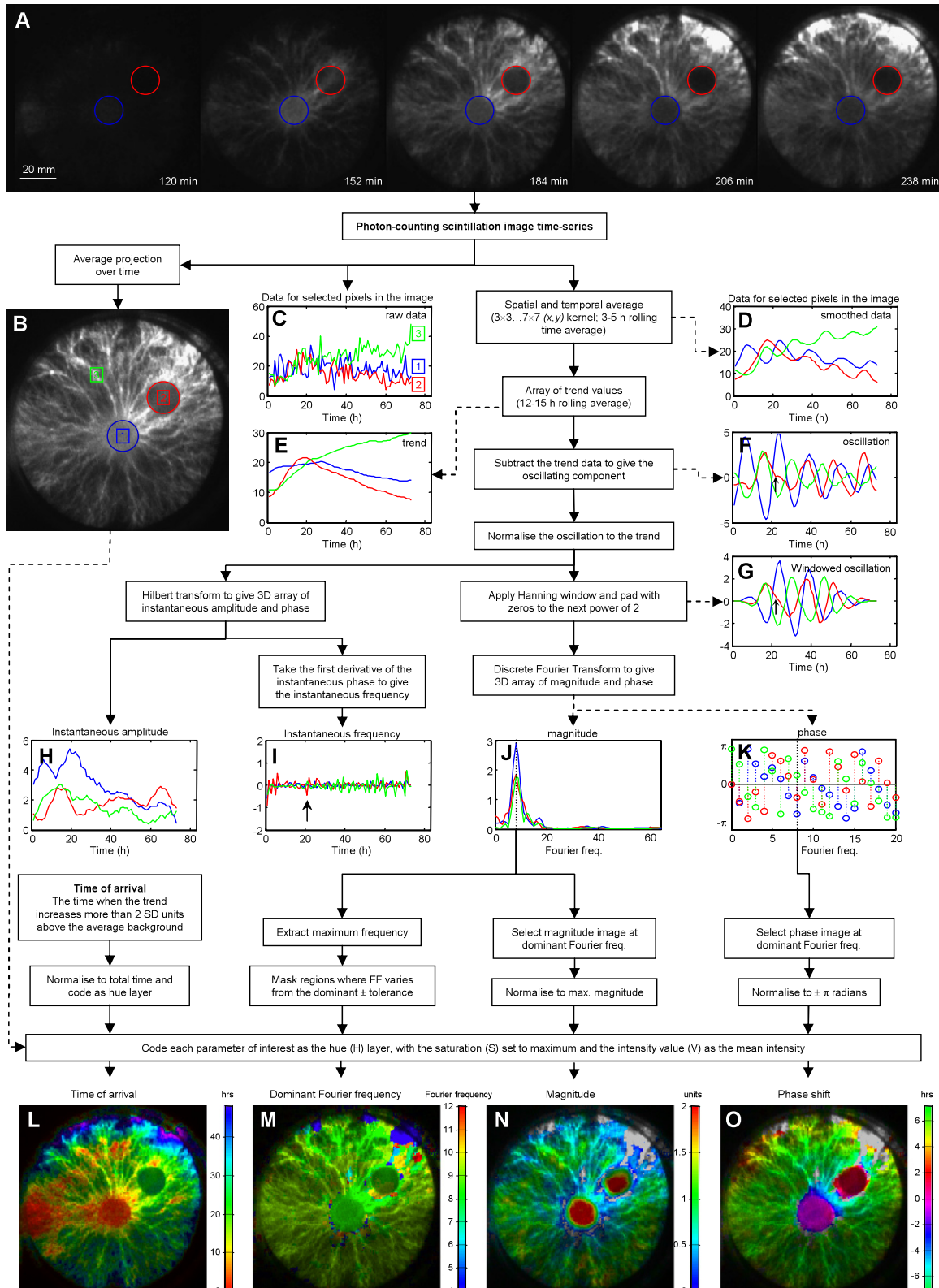
from the Hilbert transform provided the envelope of the oscillation and was often more useful than the single value derived from the Fourier analysis if the oscillation changed amplitude over the time course (Fig. 1H). In theory, the instantaneous phase should increase linearly for a simple sinusoidal oscillation. In practice, it was difficult to detect deviations from linearity in the instantaneous phase plot that might be of interest. However, the local gradient of the instantaneous phase gave a measure of changes in the instantaneous frequency (Fig. 1I Huang et al., 1999). In some cases, this provided a convenient way to detect discontinuities in the time-series. For example, if the frequency changed or there was a subtle shift in the shape of the oscillation (arrow in Fig. 1G), there was a corresponding peak in the differenced instantaneous phase signal (e.g. arrow in Fig. 1I). However, it was difficult to interpret the meaning of the instantaneous frequency unless the signal had a limited bandwidth following smoothing and de-trending and behaved as a very clean oscillation (Huang et al., 1998). Thus so far, we mainly use the instantaneous frequency response to detect whether a Fourier analysis was appropriate over the whole time-series, or whether some form of data truncation or windowing was needed.

If there were switches in behaviour or gradual shifts in the period of the oscillations, it was more appropriate to split the time-series into shorter (overlapping) segments either manually, by truncating the original data, or automatically by successively shifting a fixed aperture window over the data and analysing each segment in turn (see for example Roussel and Lloyd, 2007). Such windowed or short time Fourier (STFFT) analysis gave a series of frequency, magnitude and phase maps that evolved over time. To maintain the level of spectral resolution, the level of padding was retained. For example, in Fig. 2 two colonies of *C. puteana* grew towards each other and eventually fused (Fig. 2A). The left hand colony was labelled with [^{14}C]-AIB and showed the characteristic out-of-phase oscillation between the inoculum (I_L) and mycelium (M_L) (Fig. 2B, upper panel). The right hand colony was labelled with the non-metabolised sugar analogue, *O*-methyl glucose ([^{14}C]-OMG). The distribution pattern was slightly different to [^{14}C]-AIB, with greater accumulation at the inoculum (I_R). However, there was still an oscillatory component that differed in phase between the inoculum (I_R) and the foraging mycelium (M_R) (Fig. 2B, lower panel). Before fusion took place, the oscillations in the two colonies were independent, with clear differences in phase in the windowed time-traces (Fig. 2B) and the phase maps (Fig. 2C). Following fusion, there were surges of label between the two colonies (Fig. 2A) and the oscillations appeared to phase lock (Fig. 2D). Thus both inocula oscillated in synchrony (Fig. 2D), as did the recently interlinked mycelia, but with a phase shift of around 180°. The corresponding phase map (Fig. 2E) clearly showed the extent of the

synchronised domains and also revealed that the cord interconnecting the two inocula also formed part of the synchronised domain in the new super-colony.

3.3. Application of Fourier mapping to pulsatile growth in Physarum polycephalum

Whilst Fourier mapping provided benefits in visualisation and understanding of how nutrient transport was coordinated in mycelial networks, the approach described here is generic and can be applied to any oscillatory system that can be captured as a time-lapse grey-scale image series. To illustrate this, we analysed a completely different physiological process, namely actin–myosin based contraction waves that developed in growing colonies of *P. polycephalum*. Contractions gave rise to differences in the colony thickness that were captured in bright field transmission images. For example, changes in thickness of a micro-colony were shown by increasing intensity that shifts around the mound with time (Fig. 2F). The corresponding pseudo-colour phase map revealed that the system self-organised as two spiral contraction waves rotating in synchrony from two separate foci (Fig. 2G). During growth of larger colonies (Fig. 2H), waves of contraction became organised into discrete local domains that varied in phase between the leading edge, the developing channels and the remainder of the plasmodium (Fig. 2I). The very fine scale resolution of the phase map revealed differences in behaviour of spatially adjacent regions of the plasmodium that would be difficult to detect by any other means.

4. Conclusion and perspectives

The techniques described here provide the first level of analysis of oscillatory phenomena for systems that have important spatial structure. The use of pseudo-colour phase and amplitude maps provides a compact summary of key features of the oscillation, and is emerging as a useful strategy to visualise oscillatory behaviour in widely different domains, ranging from neuroscience (Huang et al., 2004) and cardiac imaging (Gray et al., 1998) to vegetation analysis (Moody and Johnson, 2001) and epidemiology (Rogers and Randolph, 2003). In theory this approach can be applied to any image series with oscillating signals and may useful in the microbial field to map other cyclical processes, such as conidiation (Lakin-Thomas et al., 2001; Gooch et al., 2004), synchronisation of circahoralian metabolic oscillations (Aon et al., 2007) or (circadian) gene expression patterns revealed by fluorescent or luminescent reporters (e.g. Bergero et al., 2003). In some cases, phase maps themselves may be subject to further analysis to extract regions with particular behaviour such as singularities at the centre of rotating spirals where the phase converges (Sawai et al., 2005), rotors (Gray et al., 1998) or propagating wavefronts (data not shown).

Despite the power of this approach, much of the interest in oscillations lies in understanding how these systems adjust over time as part of a developmental sequence or
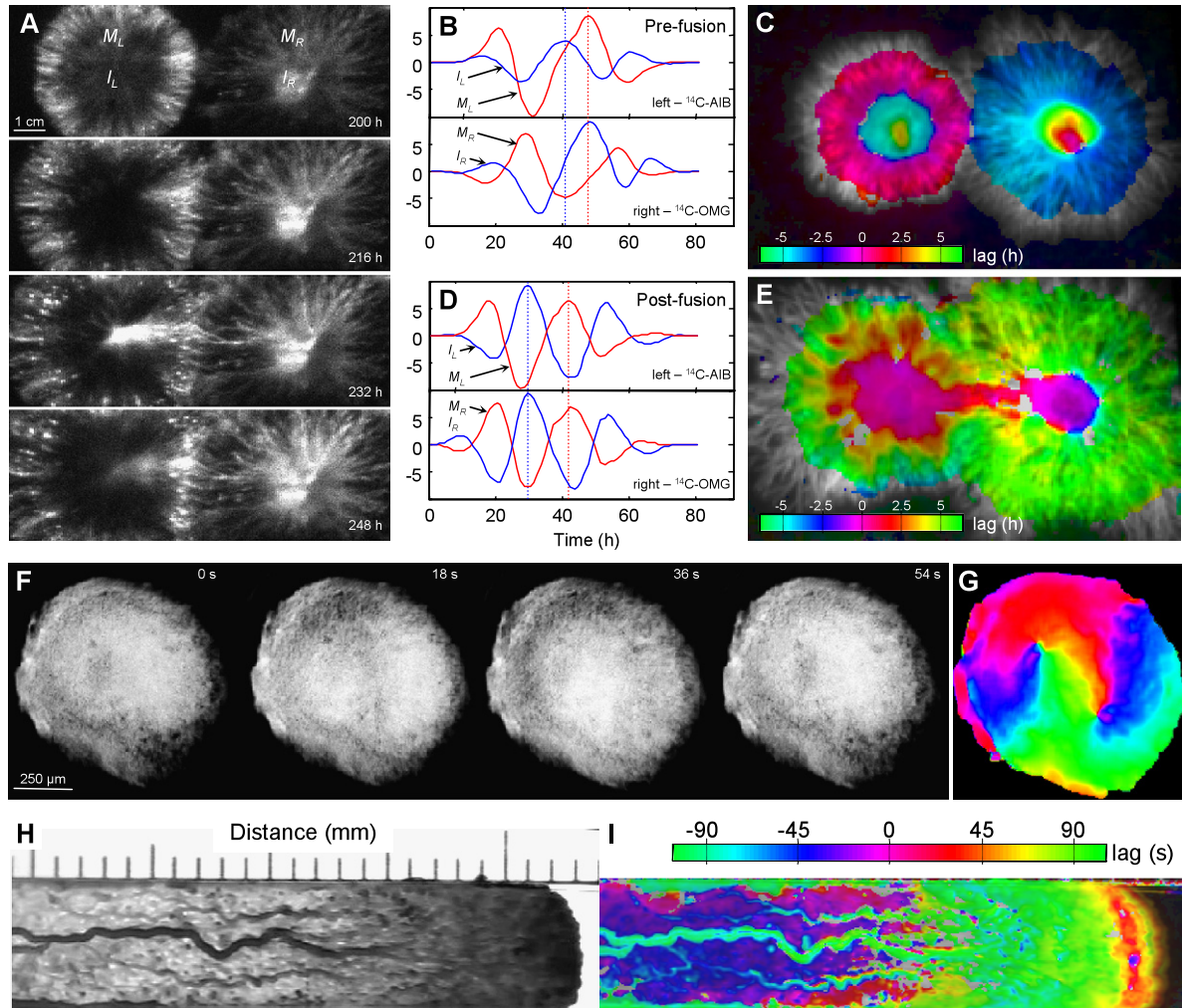
Fig. 2. Applications of phase mapping. Two adjacent colonies of *Coniophora puteana* were labelled with [^{14}C]-AIB (left) or [^{14}C]-OMG (right) and allowed to grow and fuse (A). In each colony prior to fusion, there was a substantial difference in phase between the inoculum region (I_L and I_R) and the foraging mycelium (M_L and M_R) for both [^{14}C]-AIB and [^{14}C]-OMG transport (B). The different phase relations are clearly visible in the pseudo-colour coded phase maps (C). Prior to fusion there was no synchronisation between the two colonies. Following fusion, the two inocula became synchronised, as did most of the foraging mycelia, but with a phase shift approaching 180° (D). In contrast, the phase map (E) revealed that the interconnecting cord had switched phase from the rest of the foraging mycelia, and had become phase locked almost in synchrony with the two inocula. In small droplets of *P. polycephalum*, actin/myosin based contractions set up localised spatial patterns that are visible as changes in the colony density in time-series images (F). Although waves of contraction are visible in animated time-series, the pseudo-colour coded phase map (G) provides an instant appreciation of the two interlinked rotating spirals present in this example. In growing plasmodia (H), more complex oscillations develop (I), which are organised into the advancing front (red), a sub-marginal domain fed by a series of channels (green) and intervening regions of the plasmodium (blue), all oscillating with different phases.

in response to perturbation. Thus techniques are needed that can capture both spatial-dependence and time evolution. Windowed (short time) Fourier analysis provides a useful starting point that retains the benefits of Fourier analysis, but adds some degree of temporal location (see for example Roussel and Lloyd, 2007). Wavelet decomposition provides much greater temporal localisation and provides a powerful tool to inspect the overall behaviour of specific ROIs, particularly for non-stationary signals (e.g. Le Van Quyen et al., 2001; Addison, 2005; Sawai et al., 2005). Likewise, decomposition of the signal using the Hilbert transform used here has some parallels with wavelet analysis (Le Van Quyen et al., 2001) and provides greater information on the temporal evolution of the oscil-

lation in comparison with windowed STFFT methods, particularly as it gives a convenient summary of the amplitude of the oscillation. However interpretation of the instantaneous frequency is not straightforward unless the signal has a very narrow bandwidth. In theory, Hilbert analysis can be applied to different frequency components extracted using multiple narrow bandwidth filters to achieve similar spatial and temporal localisation to continuous wavelet decomposition (see for example Le Van Quyen et al., 2001). Alternatively, Huang has developed an analysis approach for non-stationary series with the basis of the decomposition derived from the data itself, rather than by reference to correlation with defined wavelets (Huang et al., 1998; Huang et al., 1999). Thus empirical mode

decomposition (EMD) extracts a number of intrinsic mode functions (IMF) that each capture a key oscillatory component present in the original data. The Hilbert transform is then applied to each IMF to dissect out the instantaneous frequency, generating a Hilbert spectrum (Huang et al., 1998; Huang et al., 1999). For systems that do not have any previously well-characterised oscillation, the Hilbert–Huang transform may prove the most versatile extension of the current analysis approach.

Acknowledgments

References

Addison, P.S., 2005. Wavelet transforms and the ECG: a review. Physiological Measurement 26, R155–R199.

Aon, M.A., Cortassa, S., Lemar, K.M., Hayes, A.J., Lloyd, D., 2007. Single and cell population respiratory oscillations in yeast: a 2-photon scanning laser microscopy study. FEBS Letters 581, 8–14.

Bell-Pedersen, D., Cassone, V.M., Earnest, D.J., Golden, S.S., Hardin, P.E., Thomas, T.L., Zoran, M.J., 2005. Circadian rhythms from multiple oscillators: lessons from diverse organisms. Nature Reviews Genetics 6, 544–556.

Bergero, R., Harrier, L.A., Franken, P., 2003. Reporter genes: applications to the study of arbuscular mycorrhizal (AM) fungi and their symbiotic interactions with plant. Plant Soil 255, 143–155.

Chatfield, C., 2004. The Analysis of Time Series. An Introduction. Chapman & Hall/CRC Press, Boca Raton, 333 p.

Diggle, P.J., 1990. Time Series, a Biostatistical Introduction. Oxford University Press, Oxford.

Dormann, D., Weijer, C.J., 2006. Imaging of cell migration. EMBO Journal 25, 3480–3493.

Dunlap, J.C., 2006. Proteins in the Neurospora circadian clockworks. Journal of Biological Chemistry 281, 28489–28493.

Gilbert, D.A., Ferreira, G.M.N., 2000. Problems associated with the study of cellular oscillations. Cell Biology International 24, 501–514.

Gilbert, D.A., Visser, G.R., 1993. Insulin-induced enhancement of cell morphological dynamics—nonspecific biophysical mechanisms for the generalized stimulation of metabolism. Biosystems 29, 143–149.

Gooch, V.D., Freeman, L., Lakin-Thomas, P.L., 2004. Time-lapse analysis of the circadian rhythms of conidiation and growth rate in Neurospora. Journal of Biological Rhythms 19, 493–503.

Gray, R.A., Pertsov, A.M., Jalife, J., 1998. Spatial and temporal organization during cardiac fibrillation. Nature 392, 75–78.

Huang, N.E., Shen, Z., Long, S.R., 1999. A new view of nonlinear water waves: the Hilbert spectrum. Annual Review of Fluid Mechanics 31, 417–457.

Huang, N.E., Shen, Z., Long, S.R., Wu, M.L.C., Shih, H.H., Zheng, Q.N., Yen, N.C., Tung, C.C., Liu, H.H., 1998. The empirical mode decomposition and the Hilbert spectrum for nonlinear and non-stationary time series analysis. Proceedings of the Royal Society of London Series a-Mathematical Physical and Engineering Sciences 454, 903–995.

Huang, X.Y., Troy, W.C., Yang, Q., Ma, H.T., Laing, C.R., Schiff, S.J., Wu, J.Y., 2004. Spiral waves in disinhibited mammalian neocortex. Journal of Neuroscience 24, 9897–9902.

Kippert, F., 2001. Cellular signalling and the complexity of biological timing: insights from the ultradian clock of Schizosaccharomyces pombe. Philosophical Transactions of the Royal Society of London Series B-Biological Sciences 356, 1725–1733.

Lakin-Thomas, P.L., 2006a. New models for circadian systems in microorganisms. FEMS Microbiology Letters 259, 1–6.

Lakin-Thomas, P.L., 2006b. Transcriptional feedback oscillators: maybe, maybe not. Journal of Biological Rhythms 21, 83–92.

Lakin-Thomas, P.L., Brody, S., 2004. Circadian rhythms in microorganisms: new complexities. Annual Review of Microbiology 58, 489–519.

Lakin-Thomas, P.L., Gooch, V.D., Ramsdale, M., 2001. Rhythms of differentiation and diacylglycerol in Neurospora. Philosophical Transactions of the Royal Society of London Series B-Biological Sciences 356, 1711–1715.

Le Van Quyen, M., Foucher, J., Lachaux, J.P., Rodriguez, E., Lutz, A., Martinerie, J., Varela, F.J., 2001. Comparison of Hilbert transform and wavelet methods for the analysis of neuronal synchrony. Journal of Neuroscience Methods 111, 83–98.

Liu, Y., Bell-Pedersen, D., 2006. Circadian rhythms in Neurospora crassa and other filamentous fungi. Eukaryotic Cell 5, 1184–1193.

Lloyd, D., 2006. Ultradian rhythms and clocks in plants and yeast. Biological Rhythm Research 37, 281–296.

Lloyd, D., Murray, D.B., 2005. Ultradian metronome: timekeeper for orchestration of cellular coherence. Trends in Biochemical Sciences 30, 373–377.

Moody, A., Johnson, D.M., 2001. Land-surface phenologies from AVHRR using the discrete fourier transform. Remote Sensing of Environment 75, 305–323.

Mrsic-Flogel, T., Hubener, M., Bonhoeffer, T., 2003. Brain mapping: new wave optical imaging. Current Biology 13, R778–R780.

Priestley, M.B., 1981. Spectral Analysis and Time Series. Academic Press, London, 890 p.

Reinke, H., Gatfield, D., 2006. Genome-wide oscillation of transcription in yeast. Trends in Biochemical Sciences 31, 189–191.

Rogers, D.J., Randolph, S.E., 2003. Studying the global distribution of infectious diseases using GIS and RS. Nature Reviews Microbiology 1, 231–237.

Roussel, M.R., Lloyd, D., 2007. Observation of a chaotic multioscillatory metabolic attractor by real-time monitoring of a yeast continuous culture. FEBS Journal 274, 1011–1018.

Sawai, S., Thomason, P.A., Cox, E.C., 2005. An autoregulatory circuit for long-range self-organization in Dictyostelium cell populations. Nature 433, 323–326.

Smith, S.W., 1997. The Scientist and Engineer's Guide to Digital Signal Processing. California Technical Publishing, San Diego.

Tlalka, M., Hensman, D., Darrah, P.R., Watkinson, S.C., Fricker, M.D., 2003. Noncircadian oscillations in amino acid transport have complementary profiles in assimilatory and foraging hyphae of *Phanerochaete velutina*. New Phytology 158, 325–335.

Tlalka, M., Watkinson, S.C., Darrah, P.R., Fricker, M.D., 2002. Continuous imaging of amino-acid translocation in intact mycelia of *Phanerochaete velutina* reveals rapid, pulsatile fluxes. New Phytology 153, 173–184.

Ueda, T., 2005. An intelligent slime mold: a self-organizing system of cell shape and information. In: Armbruster, D., Kaneko, K., Mikhailov, A.S. (Eds.), Networks of Interacting Machines: Production Organisation in Complex Industrial Systems and Biological Cells. World Scientific, Singapore, pp. 1–35.

Visser, G., Reinten, C., Coplan, P., Gilbert, D.A., Hammond, K., 1990. Oscillations in cell morphology and redox state. Biophysical Chemistry 37, 383–394.